Spin-dependent tunneling junctions with amorphous CoNbHfFe

Manish Sharma, Lung T. Tran, Thomas C. Anthony
Benédicte Warot[1], Amanda K. Petford-Long[1]
Information Access Laboratory
HP Laboratories Palo Alto
HPL-2002-189
September 9th , 2002*

E-mail: manish_sharma@hp.com

We report on using amorphous $Co_{77}Nb_{16}Hf_6Fe_1$ (CoNbHfFe) as the ferromagnetic electrode in bottom-pinned magnetic tunnel junctions (MTJ's). Exchange bias with CoNbHfFe was achieved with $Mn_{75}Ir_{25}$ as the antiferromagnetic pinning layer. In a first sample with both pinned and sense layers being CoNbHfFe, a tunnelling magnetoresistance ratio (TMR) of 5% was found. In comparison, a TMR of 16.4% was found in a second sample with a pinned $Co_{50}Fe_{50}$ electrode and a sense CoNbHfFe electrode. This leads to a low spin-polarization of about 15% for CoNbHfFe at room temperature. High-resolution transmission electron microscopy (HREM) images show that while the first sample has a fully amorphous sense layer, the sense layer in the second sample is largely amorphous with nano-crystalline inclusions. Both pinned layers are found to be highly textured and crystalline.

To study switching distributions, large MTJ arrays were patterned using electron-beam lithography and the magneto-optic kerr effect (MOKE) was used to measure the switching of the sense layer. MOKE results for the two samples are compared in arrays with devices of different sizes.

* Internal Accession Date Only Approved for External Publication
[1] Department of Materials, University of Oxford, Parks Road, Oxford, OX1 3PH, UK

Spin-dependent tunnelling junctions with amorphous CoNbHfFe

Manish Sharma,* Lung T. Tran, and Thomas C. Anthony

Hewlett-Packard Laboratories, 1501 Page Mill Road, Palo Alto, CA 94304, USA.

Benédicte Warot and Amanda K. Petford-Long

Department of Materials, University of Oxford,

Parks Road, Oxford OX1 3PH, UK.

(Dated: September 6, 2002)

Abstract

We report on using amorphous $Co_{77}Nb_{16}Hf_6Fe_1$ (CoNbHfFe) as the ferromagnetic electrode in bottom-pinned magnetic tunnel junctions (MTJ's). Exchange bias with CoNbHfFe was achieved with $Mn_{75}Ir_{25}$ as the antiferromagnetic pinning layer. In a first sample with both pinned and sense layers being CoNbHfFe, a tunnelling magnetoresistance ratio (TMR) of 5% was found. In comparison, a TMR of 16.4% was found in a second sample with a pinned $Co_{50}Fe_{50}$ electrode and a sense CoNbHfFe electrode. This leads to a low spin-polarization of about 15% for CoNbHfFe at room temperature. High-resolution transmission electron microscopy (HREM) images show that while the first sample has a fully amorphous sense layer, the sense layer in the second sample is largely amorphous with nano-crystalline inclusions. Both pinned layers are found to be highly textured and crystalline.

To study switching distributions, large MTJ arrays were patterned using electron-beam lithography and the magneto-optic kerr effect (MOKE) was used to measure the switching of the sense layer. MOKE results for the two samples are compared in arrays with devices of different sizes.

PACS numbers: 85.75.-d,85.75.Dd,73.40.-c,75.70.-i

*Electronic address: manish_sharma@hp.com

I. INTRODUCTION

After the discovery of a large magnetoresistance effect in magnetic tunnel junctions (MTJ's) [1], they have been proposed for use as storage elements in magnetic random access memory (MRAM) [2, 3]. To compete with existing technologies, MRAM must incorporate devices with sizes 0.25 μm and less. At such small dimensions, the magnetic switching behaviour of an individual device is influenced primarily by its geometry but also by the grain structure of the magnetic layers. In particular, a polycrystalline sense layer may lead to significant variation in switching characteristics when large numbers of devices are fabricated in an MRAM array [4]. It has been proposed that the use of amorphous materials for the sense layer in an MTJ or a spin-valve improves the uniformity of switching in MRAM [4, 5]. This paper discusses the use of one such material, CoNbHfFe, as the sense layer.

II. EXPERIMENT

Samples were deposited by dc magnetron sputtering in a Sputtered Films Inc. Shamrock deposition system. The tunnel barrier of Al_2O_3 was formed by plasma oxidation of a sputter-deposited Al film. One set of samples was patterned with electron-beam lithography to form contacted bits for electrical testing and magnetoresistance measurements. Devices of rectangular shape, aspect ratio 2 and sizes down to 0.6 $\mu\text{m} \times 0.3$ μm were fabricated. Another set of samples was separately patterned to form dense arrays of devices of rectangular and elliptical shapes with an aspect ratio of 2.5 and sizes down to 225nm $\times$ 90nm. This set was used for observing magnetic switching behaviour of the sense layer using MOKE measurements. HREM was performed on a set of witness samples to study the multilayer structure in detail.

In this paper, data from two samples are presented: Sample 1, with Ta 3/ Ru 2/ MnIr 7.5/ CoNbHfFe 3/ Al_2O_3 2/ CoNbHfFe 5/ Ta 5, and Sample 2, with Ta 3/ Ru 2/ MnIr 7.5/ CoFe 2/ Al_2O_3 2/ CoNbHfFe 5/ Ta 5 (where thicknesses are in nm). Thus, the two samples differ only in the material used for the pinned layer. CoNbHfFe has a moment of 850 emu/cc, close to Permalloy ($Ni_{80}Fe_{20}$), and has a high enough Nb and Hf content to be amorphous in thin film form. The sense layers are expected to be very similar in structure, being amorphous films deposited on amorphous alumina. However, as discussed below, they are found to be different.

III. RESULTS AND DISCUSSION

Fig. 1 shows observed R-H loops for rectangular junctions of 1.50 μm $\times$ 0.75 μm size. The TMR for Sample 1 is 4.9% and for Sample 2 is 16.4%. Using the Julliére definition for spin polarization [6], these TMR values suggest a spin polarization of around 15% for CoNbHfFe at room temperature. The exchange bias in Sample 1 with CoNbHfFe pinned layer is 225 Oe and in Sample 2 with CoFe pinned layer is 350 Oe.

In Fig. 2 are presented HREM images of the two samples. Surprisingly, both pinned layers are found to be predominantly crystalline and highly textured. The crystalline structure of the CoNbHfFe pinned layer explains the observation of exchange bias in Sample 1. Due to texture already established by the underlying MnIr, the CoNbHfFe layer does not seem to grow amorphous, although some small amorphous regions are still observed (Fig. 2(a)). The degree of texture in the pinned CoFe layer in Sample 2 is higher. In looking at the sense layer of Sample 1, a fully amorphous CoNbHfFe layer is observed. However, the sense layer of Sample 2 is found to have a significant proportion of crystalline regions. This is unexpected as both the sense layers are grown on amorphous alumina. The alumina barrier does not seem to fully break the texture established by the bottom electrode layers and some of it propagates into the top electrode.

In trying to understand the differences between the two sense layers, we prepared large arrays to compare by MOKE measurements. To get acceptable statistical distributions of switching, one requires identical devices in the entire array. An important goal of the patterning process was to keep shapes and sizes of all devices in an array similar. Devices were spaced far apart to be non-interacting. Fig. 3 shows a scanning electron microscope (SEM) image of a typical MOKE array of ellipses.

Representative M-H loops for rectangles measured by MOKE are also plotted in Fig. 1. A feature evident is the stepped transition in one of the edges. This was frequently observed in electrical and MOKE data from rectangular bits, but not in ellipses. The steps are likely related to formation of vortices and other effects that are known to affect switching in rectangles more than in ellipses [7, 8].

In Fig. 4 are plotted MOKE data for ellipses. As expected, coercivity increases substantially as bit size decreases (cf. Fig. 5(a)). Two differences exist between Samples 1 and 2. First, the increase in coercivity is smaller for Sample 2. Second, a significant tail is seen in Sample 2 at small sizes and only in transitions from parallel to antiparallel. As individual bits in the array switch at slightly different coercivities, the slope dM/dH gives the switching distribution with standard deviation σ (for a Gaussian fit). The tail in Sample 2 causes the normalized coercivity spread, σ/H_c, to increase for one of the edges (see Fig. 5(b)). Since the primary difference between the two samples is the crystallinity of the sense layer, these two differences suggest a link between texture and switching distribution. Additional contributing factors could be the influence of the different pinned layers due to local dispersions in pinned layer orientations and different pinning field strengths [9].

IV. CONCLUSION

In summary, tunnelling magnetoresistance has been observed in junctions with CoNbHfFe electrodes, although observed TMR values suggest a low spin polarization of 15% for CoNbHfFe. Exchange bias was observed for MnIr/CoNbHfFe layers. HREM images confirmed that such CoNbHfFe pinned layers were not amorphous but largely crystalline. In comparing HREM images of two samples with different pinned layers, it was clearly seen that the structure of the amorphous material is influenced by the underlying layers and their texture. Depending upon its position in the TMR multilayer stack, the same material may be amorphous or crystalline to varying degrees. The amorphous alumina barrier apparently does not fully break the texture established by underlying layers. When patterned into MRAM arrays, the two samples showed different switching behaviour. The switching was similar at dimensions above 500nm but increasingly different at dimensions below 200nm. This suggests that the degree of crystallinity of the sense layer affects the magnetic switching of bits.

Acknowledgments

The authors would like to thank Michelle Pangborn for her great help with the MOKE measurements.

[1] J. Moodera, L. Kinder, and J. Nowak, J. Appl. Phys. **81**, 5522 (1997).

[2] W. Gallagher, S. Parkin, Y. Lu, X. Bian, A. Marley, R. Altman, S. Rishton, K. Roche, C. Jahnes, T. Shaw, et al., J. Appl. Phys. **81**, 3741 (1997).

[3] S. Tehrani, J. Slaughter, E. Chen, M. Durlam, J. Shi, and M. DeHerren, IEEE Trans. Magn. **35** (1999).

[4] H. Kano, K. Bessho, Y. Higo, K. Ohba, M. Hashimoto, T. Mizuguchi, and M. Hosomi, IEEE Trans. Magn. **38** (2002).

[5] D. Wang, Z. Qian, J. Daughton, C. Nordman, M. Tondra, D. Reed, and D. Brownell, J. Appl. Phys. **89**, 6754 (2001).

[6] M. Jullière, Phys. Lett. **54A**, 225 (1975).

[7] T. Schrefl, J. Fidler, K. Kirk, and J. Chapman, J. Magn. Magn. Mater. **175**, 193 (1997).

[8] R. Gomez, A. Pak, V. Luu, K. Kirk, and J. Chapman, J. Appl. Phys. **85**, 6163 (1999).

[9] C. Tiusan, T. Dimopoulos, K. Ounadjela, M. Hehn, H. van den Berg, V. da Costa, and Y. Henry, Phys. Rev. B **61**, 580 (2000).

FIG. 1: Comparison of electrical R-H data (solid line) with MOKE loops (dashed line) for rectangular bits. Magnitude of MOKE signal along y-axis is only relative.

FIG. 2: HREM images of (a) Sample 1 with CoNbHfFe pinned layer, and (b) Sample 2 with CoFe pinned layer. In (b), a crystalline region in the sense layer is circled.

FIG. 3: SEM image of a MOKE array with 400 nm $\times$ 200 nm ellipses at a pitch of 800 nm $\times$ 400 nm patterned by electron-beam lithography.

FIG. 4: MOKE loops for elliptical bits with aspect ratio of 2.5. Minor axis dimension is indicated for devices.

FIG. 5: Effect of device size on (a) coercivity, H_c, and (b) normalized coercivity spread, σ/H_c, for elliptical bits. In (b), the two M-H loop edges are plotted separately.

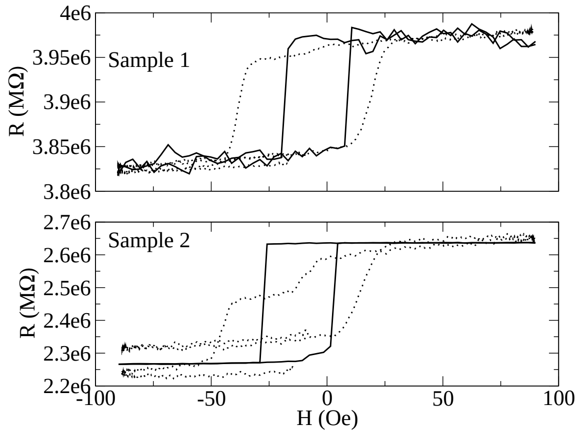
Sample 1
Sample 2
R (MΩ)
H (Oe)
4e6
3.95e6
3.9e6
3.85e6
3.8e6
2.7e6
2.6e6
2.5e6
2.4e6
2.3e6
2.2e6
-100
-50
0
50
100

FIGURE 1

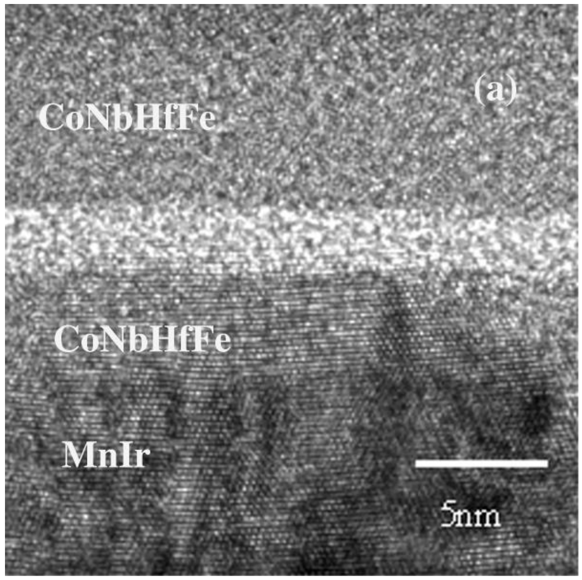

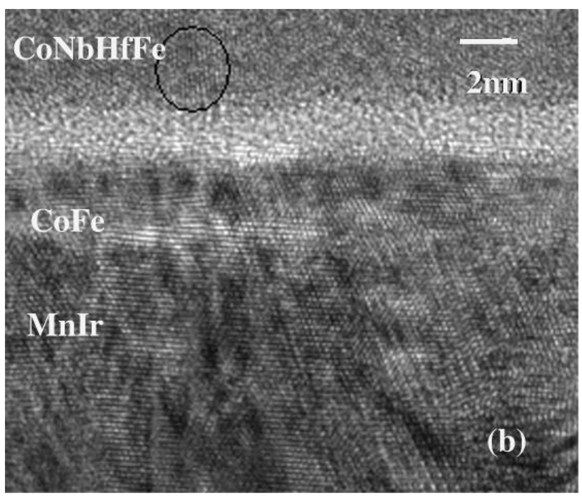

FIGURE 2

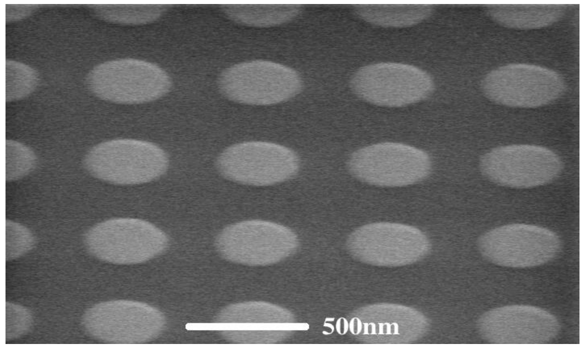

FIGURE 3

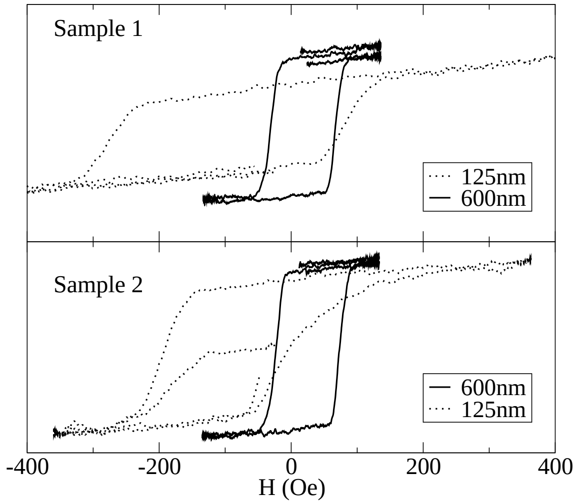
Sample 1
125nm
600nm
Sample 2
600nm
125nm
-400
-200
0
200
400
H (Oe)

FIGURE 4

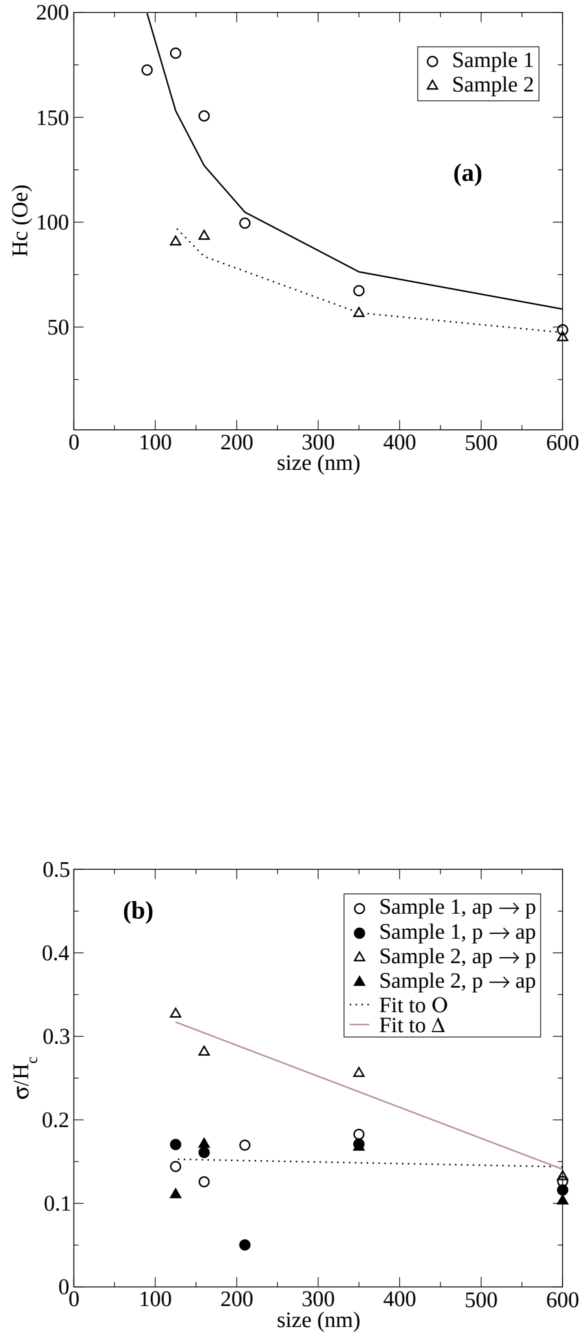
200
150
100
50
Hc (Oe)
0
100
200
300
400
500
600
size (nm)
Sample 1
Sample 2
(a)
0.5
0.4
0.3
0.2
0.1
0
σ/H
c
(b)
Sample 1, ap → p
Sample 1, p → ap
Sample 2, ap → p
Sample 2, p → ap
Fit to O
Fit to Δ

FIGURE 5